Marinizing the Sensor Web

Samareh Attarsharghi

Vlastimil Masek

Attarsharghi and Masek continue their journey in pursuit of a practical approach to monitoring ocean currents over large areas.

Who should read this paper?

Oceanographers or researchers with an interest in the practical aspects of deploying an underwater sensor network.

Why is it important?

The term "sensor web" was first coined by NASA in the late 1990s to describe a network of spatially distributed sensor platforms or "pods" that communicate with each other. Pod-to-pod communication was viewed as being both omni- and bi-directional and thus each pod would be in contact with every other pod in the network at all times. The NASA definition of a sensor web was that of an autonomous entity that would not necessarily require the presence of the World Wide Web to function. More recently, the Open Geospatial Consortium (OGC) has re-defined "sensor web" as an infrastructure that enables access to sensor networks and data using standard Web protocols and application programming interfaces. The OGC Sensor Web Enablement initiative defines the service interfaces which will enable an interoperable usage of sensors by facilitating their discovery, access, interrogation and control.

The authors have devised a sensor web approach to monitoring and measuring ocean currents over large areas based on a call-response network of acoustic transducers. In a previous paper (JOT Vol. 11, No. 1) the first author described a large-scale system design, then used simulation to test the effectiveness of the design. In this paper, the focus is on refining the network topology and architecture with an eye towards maximizing the energy efficiency of the network as a whole. This is a practical consideration given the challenges of generating and managing power in a remote subsea environment.

The authors see particular benefits of their proposed approach for the Arctic region, where a bottom-mounted, energy efficient acoustic sensor web could be used to monitor the long-term effects of climate change on regional and local current patterns.

About the authors

Samareh Attarsharghi is a doctoral candidate at Memorial University of Newfoundland. Her area of study is underwater acoustic sensor networks. She is currently developing new architectures of acoustic sensor networks for ocean current monitoring which are optimized in terms of energy consumption and coverage area. Vlastimil Masek is an Associate Professor in the Faculty of Engineering and Applied Science at Memorial University of Newfoundland and a licensed Professional Engineer. His research interests include multiphase flow sensing and in-flow phase separation, oil spill remediation, wide area ocean current sensing, and seabed instrumentation networks.

ENERGY EFFICIENT ARCHITECTURE DESIGNS OF AN UNDERWATER ACOUSTIC SENSOR NETWORK FOR OCEAN CURRENT MONITORING

Samareh Attarsharghi and Vlastimil Masek
Faculty of Engineering and Applied Science, Memorial University of Newfoundland, St. John's, NL, Canada

ABSTRACT

Providing energy to an underwater sensor network has always been a challenge due to the rough condition at sea as well as the lack of access to deployed equipment for battery replacement. Moreover, the lack of solar energy excludes the use of solar cells in cold oceanic regions. In such harsh conditions, maximizing sensors' life time is an essential goal.

In the area of ocean current measurement, some of the existing methods are mostly limited to measure only the surface current and not the shallow water current, while some other methods measure the speed of water in a vertical column only at one location. There are other systems that measure and store the current data of different locations and depths over time (few days) so the current data saved in them are not real-time. This study aims to overcome some of these limitations and proposes a real-time measurement method for wide area averaged current. Thus, in this paper, novel underwater sensor network topologies and architectures have been designed and proposed.

These new proposed architecture designs specifically aim to maximize the network lifetime by minimizing the energy demand of the whole network. For this purpose, two types of network topologies, Hexagonal and Square, with two different configurations of with- and without-centre node for each type, have been designed and offered. The method used in the current measurement networks is based on transit time method and could be considered a modified version. Using the new modified measurement method, these novel architecture designs unravel the limitations of the existing current measurement methods. In this paper, the proposed architecture designs' performance has been compared to each other and also their pros and cons have been discussed.

KEYWORDS

Underwater acoustic sensor networks (UASNs); Energy efficiency; Acoustic sensor network; Network architecture; Network topology

INTRODUCTION

Underwater sensor networks provide robust communication for many applications such as underwater data collection, navigation, prevention of disasters, etc. One of the network's applications could be precise monitoring of the ocean current. Ocean current measurements are specifically important to both ocean related industries and researchers because the currents affect the global climate [NOAA, n.d.A.], work in favour or against the marine transportations, carry nutrients [NOAA, n.d.B.] or steer icebergs [Eik, 2009; Turnbull et al., 2015].

In order to obtain a vast area real-time measurement of the ocean current, different architecture designs of acoustic sensor networks are proposed. Acoustic sensors are used in this study because sound waves can propagate through the ocean layers over a large distance [Urick, 1983]. The absorption of sound in water depends on its frequency and if the frequency is sufficiently low (e.g., 57 Hz) then sound can propagate thousands of kilometres (18,000 km) [Brekhovskikh and Lysanov, 2003].

Existing methods of ocean current measurement such as remote sensing methods, acoustic Doppler current profilers (ADCPs) and Argos all have limitations for wide-area real-time shallow water current measurement. For example, remote sensing techniques (e.g., satellite and radar) only provide the surface current measurements [Dohan and Maximenko, 2010; Paduan and Washburn, 2013]. ADCPs, on the other hand, measure a point nature profile data of the ocean current. As well, their directional accuracy depends on the accuracy of compass readings. Finally Argos yield the current data which is not real-time because they travel deep under the water for several days before the data stored in them can be downloaded [Fossette et al., 2012]. As a result, a novel proposed current monitoring technique in this paper aims to overcome these limitations.

The proposed technique in this paper is based on transit time method [Lynnworth, 2013]. The transit time method is actually used for measuring the speed of sound in water while collecting ocean current features. Computing the speed of sound will be the first step of the proposed current measurement method; called the self-calibration phase (step). The importance of this phase is explained in detail in "Structure of the Novel Architecture Design for Current Measurement Underwater Networks." Then, in the next step the arrangement of the acoustic sensors in a network is addressed. As an introduction to the networks and deployment methods, a review is done on the deployment algorithms. Han et al. [2013] have divided deployment algorithms into three groups of static, self-adjustment and movement-assisted deployment (also called dynamic deployment). The static deployment is considered in this work.

Static deployment is the one which is of interest in this research because this technique results in a two dimensional deployment and therefore in saving energy. In fact, the number of nodes for achieving an acceptable coverage in a three-dimensional network is excessively higher than the two-dimensional network which will result in higher energy consumption and more costs. An example would be the

three-dimensional network in Xiaoyu et al. [2013]. Therefore static topology, which forms a two-dimensional network [Han et al., 2013], is the proper design for horizontal ocean current monitoring that meets energy saving requirements. Therefore, neither the self-adjustment nor the movement-assisted deployments are the target in this paper as they might result in three-dimensional networks. In fact, for some specific applications of ocean current monitoring, such as iceberg trajectory predictions, a three-dimensional network is not desirable because a horizontal-section-averaged vector of the current is needed and not a vertical-column-averaged vector.

In terms of dynamic deployment, it should also be mentioned that this kind of deployment is not desirable because moving devices, such as Argos, go to a depth of up to 2,000 metres under the water [NOAA, n.d.C.] and drift for up to 10 days and then come back to the surface to communicate wirelessly to shore. Therefore, not being a real-time system is a drawback of the current measured by these devices. Furthermore, Argos can sometimes be lost or difficult to track especially in harsh sea conditions.

Autonomous underwater vehicles are another example used in dynamic deployment which are popular [Mitra et al., 2015]. In addition to not yielding a real-time measurement, they are very expensive with high costs associated with their maintenance and fuel.

In order to save energy within the network, another strategy is to maximize the network coverage, which is also an important target of this study. The proposed techniques in the new designs of the network aim for a larger area to be covered by fewer acoustic sensors in order to keep energy demand as low as possible.

In order to reinforce the importance of the power provision for instruments in open water, it should be mentioned that many reports have strived to overcome the limitations of energy in underwater acoustic sensor networks (UASN). Heidemann et al. [2012] reported the power consumption issue in UASNs through protocol. Another example is in Hu and Fei [2010] who suggest an adaptive routing algorithm to achieve an energy efficient UASN. Underwater communication protocols and routing algorithms are techniques to deal with data communication challenges. For underwater monitoring applications, which is the intent of this research, a novel approach is offered in this paper that could solve the problem of energy deficiency in UASNs efficiently and with less complexity. Minimization of energy consumption in an UASN with data transmission application (which needs a high rate of transaction of data) is different from a network with monitoring purposes (which might need to run once or twice an hour or even less frequently) in terms of topology and architecture design. Challenges faced in designing these two types of networks are different in nature.

Jha et al. [2015] address a surveillance network energy management (which is a type of data transmission application) where optimization of topology is advised by using genetic algorithm. Jha et al. [2015] give a target detection model, network connectivity and protocol model, and solve the target detection problem by the equations defined in

the modelling. Researchers also proposed a design on data transmission networks in which power consumption to throughput ratio [Tilak et al., 2002; Etter, 2013] and spectrum allocation [Jurdak et al., 2004; Jornet et al., 2010] are the parameters which play an important role in the design of the network.

On the other hand, in monitoring application networks, throughput ratio (the rate at which information is transferred) and update period of data is not important because the whole system is run less frequently. Among the literature [Jurdak et al., 2004] is one of the pioneer examples that has addressed the topology of the UASN in order to maximize the network's lifetime. Although the authors use transmission frequency and update period as their design factors, they also use transmission distance and number of nodes in a cluster, which is applicable in a monitoring application network design. Therefore the present study offers a new scheme by using the concept of increasing transmission distance and reducing the number of nodes in order to minimize energy consumption in the whole network.

Finally, there are important facts that should be mentioned here about the differences between the underwater communication environment and the terrestrial environment. The cost of the deployment and the power demands [Xiao, 2010] are the two significant differences of the terrestrial and underwater networks.

These have been the underlying motivations to conduct meaningful research on a novel underwater architecture design in this study. The rest of this paper is organized as follows.

In the next section, details about the structure of the basic blocks forming the new network architectures are explained. These novel architecture designs contribute to a longer lifetime of the network in order to overcome the dissipation of energy. "Comparison of the Performance of Two Architecture Designs" provides an in-depth analysis of the factors affecting the acoustic modem energy consumption in the proposed energy-efficient UASN, such as coverage area and node density. A graphical comparison has also been provided in order to distinguish differences among the proposed designs. At the end, "Conclusion" is provided along with a future work plan.

STRUCTURE OF THE NOVEL ARCHITECTURE DESIGN FOR CURRENT MEASUREMENT UNDERWATER NETWORKS

The design of the current measurement networks is based on experimental results described in [AquaTrans, n.d.]. A schematic of the lab-scale prototype of the current

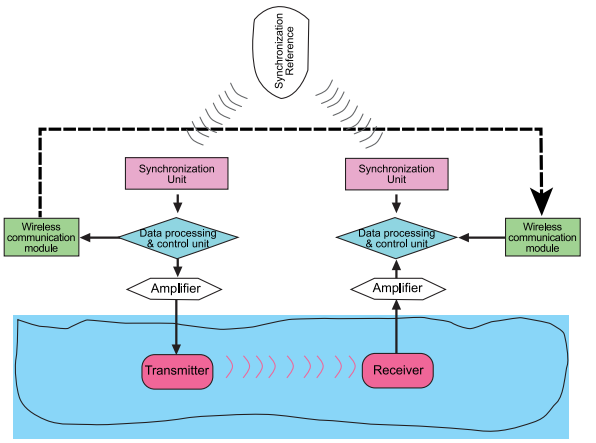

Figure 1: Current measurement system block diagram. The wireless modules are Zigbee wireless unit, GPS is the synchronization unit. Calculations and algorithms are implemented and performed with the Arduino microprocessor.

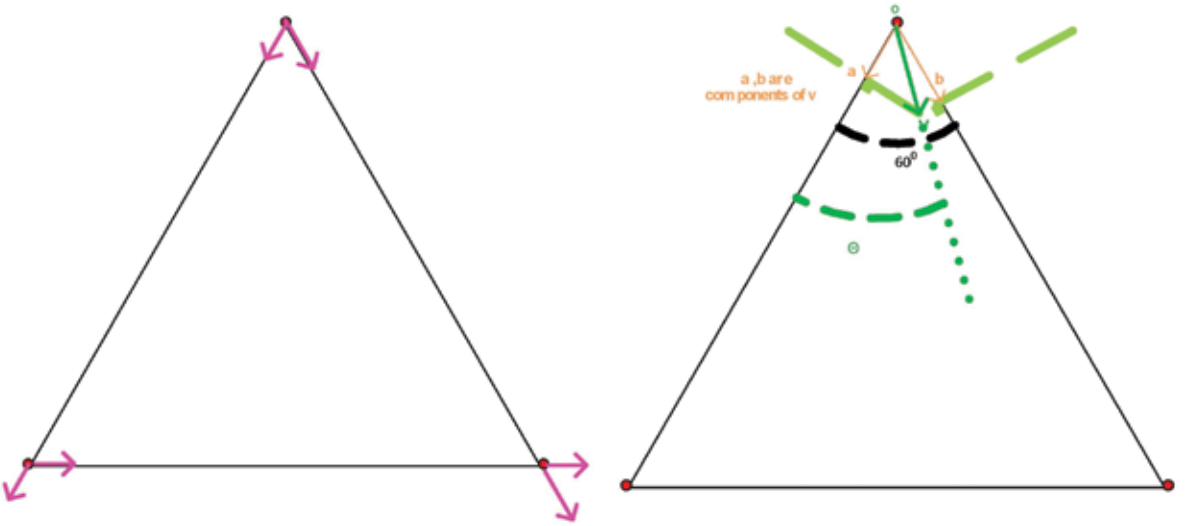

Figure 2: Left: Basic cell for measuring the current vector. The two vector components, shown on each vertex, are measured during the process of measurement. Right: The resultant vector, *V* [m/s], is the original current vector that its components (vectors a and b) are measured on the vertex.

measurement system is sketched in Figure 1. The experiment uses transit time method and cross correlation technique along with the synchronization of two nodes. As mentioned above, this forms a fundamental block of the design of an expanded network for larger scale implementation.

Principles of the network design are as follows. The acoustic nodes actually form basics cells of three or four nodes to measure the average vector of the shallow water current. In Figure 2, the procedure for the three-node-design is depicted. The vector of current is measured between each two nodes in Figure 2 (left). These two vectors are the components of a main current vector that is shown in Figure 2 (right). The resultant vector's magnitude and direction are given by Equation (1). The experimental setup details including drivers and amplifiers design and the result of calculations in the microprocessor are explained in Attarsharghi and Masek [2014].

A two node system (fundamental setup) was experimentally validated and thus can form a basis for a large scale shallow current measurement system.

The Basic Design: Without Centre Node

In Figure 2 (left), the magnitudes of vectors *a* and *b* are given from the measurements. Since the placements of nodes are on the vertex of an equilateral triangle, the angel on each vertex is 60º. According to the Figure 2 (right), the angle θ should be found from Equation (1) in order to find the magnitude of the resultant vector *V* [m/s]. The resultant current vector's (V) direction is then θ [º] relative to the direction of the vector *a*.

$$V = \frac{a}{cos\theta} \; or \; V = \frac{b}{\cos(90°-\theta)} = \frac{b}{sin\theta} \qquad (1)$$

$$\frac{\mathrm{Cos}(60°-\theta)}{cos\theta} = \frac{b}{a},$$

In which:

$$\cos(60° - \theta) = [(cos60°)(cos\theta) + (sin60°)(sin\theta)]\,|\; if\ divided\ by\ (cos\theta);then$$

$$cos60° + (sin60°)(tan\theta) = \frac{b}{a}, tan\theta = \frac{\frac{b}{a} - cos60°}{sin60°},$$

$$\theta = \arctan\left(\frac{\frac{b}{a} - cos60°}{sin60°}\right)$$

$$V' = \sqrt{a^2 + b^2} \tag{2}$$

$$\theta' = \tan^{-1}\frac{a}{b}$$

As the process of measurement was described in Figure 2 and for a network with Triangle topology, each node in the vertex of the basic cell is once a transmitter and twice a receiver. So there are two velocity vectors at each vertex that are added together to yield the average vector of the current.

This triangular topology is compared with a Square topology. The procedure described for triangular topology can actually be performed for the Square topology which is described in Figure 3. The Triangle and Square designs of the network map the current of the target area with three and four separate vectors, respectively.

The resultant current vector's (V' [m/s]) direction (θ' [°]) is relative to the direction of the vector b.

In this section, the basic blocks of the UASN, which are a combination of either three or four acoustic sensor nodes, have been introduced. In the above introduced basic cells, transit time method is the principle of current measurement. Using the transit time between each pair of acoustic nodes, the average current will be measured. All nodes using this principle of measurement need to

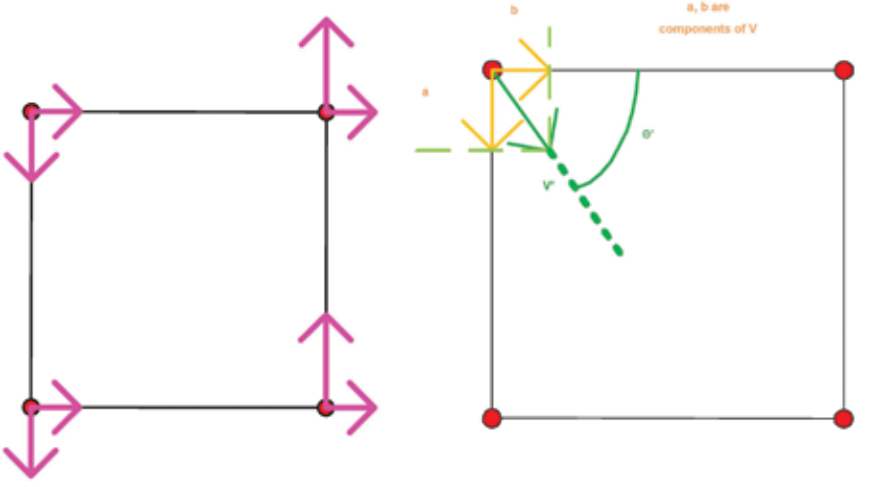

Figure 3: Left: Square basic cell for measuring the current vector. The two vector components, shown on each vertex, are measured during the process of measurement. Right: The resultant vector, *V* [m/s], is the original current vector that its components (vectors a and b) are measured on the vertex.

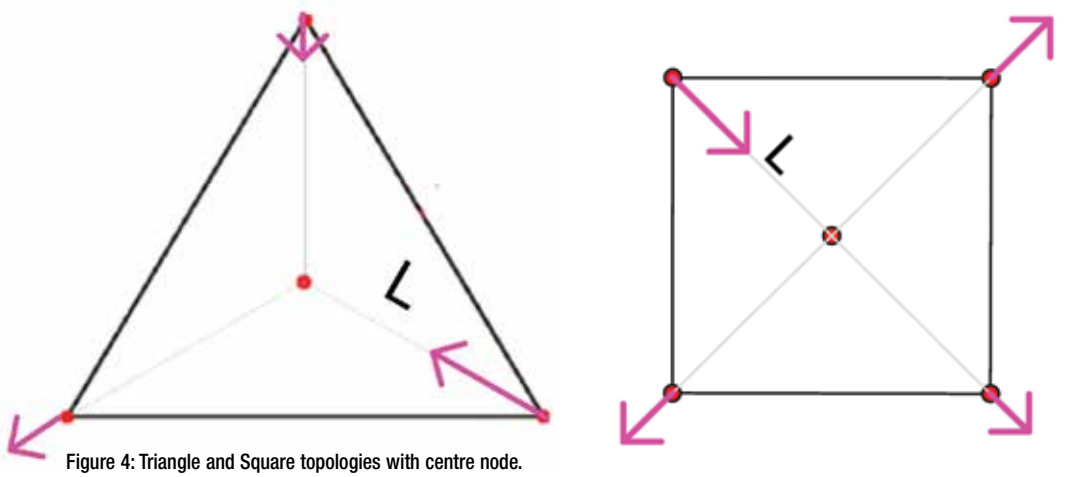

Figure 4: Triangle and Square topologies with centre node.

be once a transmitter and another time a receiver. The transmitters' power consumption is the main concern, as they use a significant amount of the energy in the underwater environment. Therefore, another method, which is a modified version of the transit time method, along with new basic blocks, is proposed in this paper. In the new proposed configurations an additional node is added in the centre of each of the above configurations. This addition converts the nodes in the vertices of the basic blocks to receivers and only the centre node is a transmitter. This way energy consumption is reduced considerably. In the next sections, details of the development of new architecture designs as well as their pros and cons are explained.

With a Centre Node Architecture Design

In order to make the underwater network sustainable in large scale, this papers offers new architecture designs.

Instead of measuring the current between the two nodes on the vertex, the current is measured between each vertex and the centre node in the new architecture (Figure 4). Traditionally a node at each vertex is both receiver and transmitter. In the proposed design, the centre node (in both Triangle and Square design) is the only transmitter (which consumes more energy than the receiver) and other nodes in the vertices are all just receivers. The travel time of underwater acoustic signals is measured at the receivers in the vertices, and thus the current vectors are calculated at the vertex nodes (receiver nodes). These calculated vectors are collected by the centre node to be sent to shore. The centre node can also do the summation and averaging of the vertices vectors and send them to shore. Therefore, in this topology (with-centre-node), sound waves only travel a single direction (despite the transit time in which waves need to travel in two directions) and thus the number of transmitters for each measurement is reduced from two transmitters to just one and thus energy consumption which is mainly demanded by the transmitters is reduced considerably [Lynnworth, 2013; Attarsharghi and Masek, 2014]. The principle of using this method is based on Equation (3) in which V [m/s] is the velocity of the current to be measured, C [m/s] is the speed of the sound which is considered to be determined by a new phase added in the process of measurement

called the self-calibration method, t_{up} [s] and t_{down} [s] are the two time readings, and L [m] is the distance between two nodes.

According to Equation (3), whether the sound travels upstream (t_{up}) or downstream (t_{down}), the speed of the sound (C) in the vicinity of the nodes is needed for the current vector (V) calculations.

$$V + C = \frac{L}{t_{up}} \qquad C - V = \frac{L}{t_{down}} \tag{3}$$

The self-calibration phase is introduced in this paper as a solution to measure C which is described in the next section.

Self-Calibration Phase for the Cells With-Centre-Node

In order to measure the speed of the sound (C), which is needed in the calculations of water velocity, the calibration phase is introduced. Calibration phase is defined as the procedure of transmitting the acoustic signals between a vertex and the central node in a cell (Figure 5)

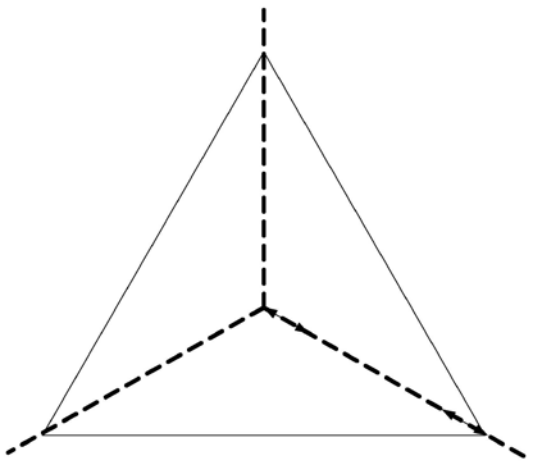

Figure 5: Calibration phase.

and calculating the speed of sound at the time of the measurements and in vicinity of the active nodes. This phase empowers the whole network to avoid extra calculations and consequently energy consumption. Equation (4) explains how the value of C is calculated using t_{up} and t_{down}.

$$t_{up} = \frac{L}{(c+v)} \qquad t_{down} = \frac{L}{(c-v)} \qquad C = \left(\frac{L}{2}\right)\left(\frac{t_{up}+t_{down}}{(t_{up})(t_{down})}\right) \tag{4}$$

The calibration phase, actually, does not need to be done in all of the basic cells and can only be done in one basic cell in a large area, depending on how accurate C is needed to be considered in a region. Knowing the value of C, by using Equation (3) the value of V is obtained. Therefore, as can be seen, this phase reduces the necessity of having a transmitter circuitry in all vertices. In the calibration cell, the centre node needs to have both receiver and transmitter circuitry. This is how the calibration phase helps with mitigating the power consumption of the whole network. The bigger area C can be considered to be constant, the fewer calibration cells are needed and therefore the more energy is saved.

After the calibration phase, the magnitude of the velocity vector is computed at each vertex by Equation set (3) and is reported to the centre node of each cell. Then at the centre node, these magnitudes, which are the components of the main current vector, are added together (similar to the procedure in Figure 2 right and Figure 3 right). Thus the

resultant vector (direction and magnitude) obtained by this procedure at the centre node is the average velocity vector of the water in the area that the cell covers.

COMPARISON OF THE PERFORMANCE OF TWO ARCHITECTURE DESIGNS

This section elaborates on the advantages of new architecture design (with-centre-node) with extended inter-node distance and smaller node density and the effects on the main goals which are energy consumption and area coverage. But before that, the structure of the networks is explained which are constructed by the triangular or Square basic cell. It should be mentioned that in the without-centre-node configuration the method used for current measurement is the traditional transit time method between each pairs of nodes. While in the with-centre-node configuration, the novel proposed method is used, which needs a calibration phase for determining the underwater sound speed in a desired area and after obtaining the sound speed, the water current speed can be measured.

In Figure 6, grids (networks) of combined basic cells (Triangular- and Square-cells) are sketched. In the next sections, the Square and Hexagon designs will be compared to each other in terms of coverage and node density.

As it can be seen in Figure 6 (b) and (e) in order to avoid the overlap of coverage of adjacent basic cells and also to avoid the waste of energy in the whole grid, every second H- or S-cell in the extended grid needs a centre node and not all of the cells have a centre node. In fact the redundant sensors are

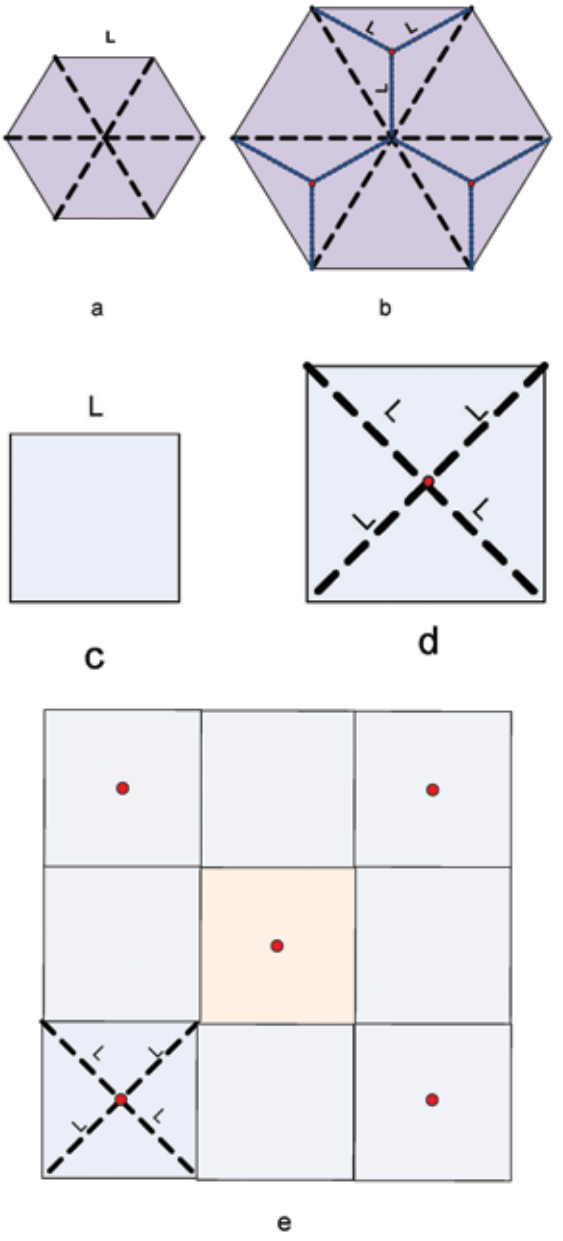

Figure 6: Hexagon-cells consisting of six triangular-cells: (a) Basic-triangular-cells without centre node. (b) Hexagon-cells (H-cells) with centre node. Square-cells consisting of one Square-cell either (c) basic Squares without centre node or (d) big-Square-cells (S-cells) with centre node which is an extended form of the basic Square cell. The red small circles represent the centre acoustic nodes which are the transmitters. Figure (e) demonstrates two layers of the big-Square-cells network consisting of S-Cells. In order to avoid redundant calculations, every second H- or S-cell has the centre node and not all of the cells have a centre node.

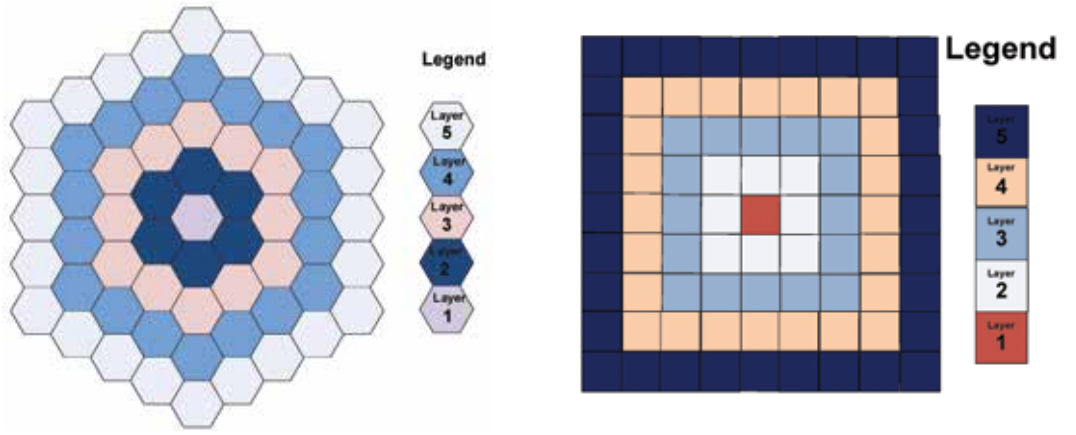

Figure 7: Two-dimensional wide area network configuration consisting of H-cells (on the left side of the figure) and S-cells (on the right side of the figure). Legends show the number of the layers.

eliminated in the grid. Omitting the redundant sensors results in less energy consumption as well. Figure 7 shows the two dimensional grids with several layers of H- and S-cells.

In the following sections, and according to the two types of H- or S-cells introduced above, they will be referred to as with-centre-node representing the new proposed design and without-centre-node representing the basic design. According to these two types of grids, the tables are set and equations are derived. It should be mentioned that the inter-node distance (L) in the designed UASNs is limited in length (to 3.2 km, in this paper, which is used for evaluation and comparison of the UASNs' performance) by attenuation of the electromagnetic waves. Electromagnetic waves are sent by ZigBee module (Figure 1) and used for synchronizing the transceivers in the designed network. Details about the synchronization process and the length limit are explained in Attarsharghi and Masek [2014] and Attarsharghi [2016].

The first subsection explains the coverage area achieved by each of the architecture designs.

Coverage

In order to examine the coverage of the network's parametric equations of the area, coverage of the basic cells are presented and compared together.

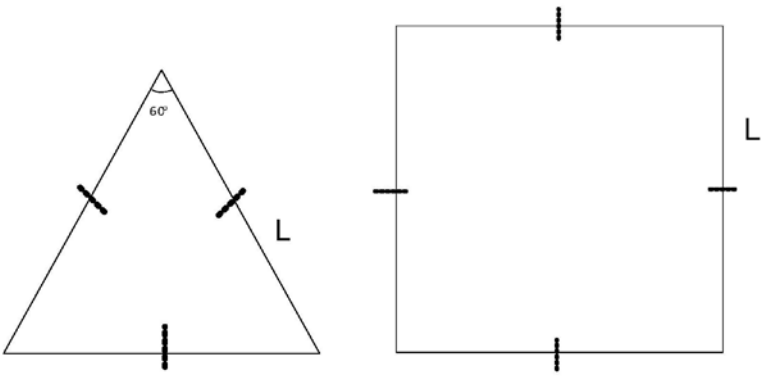

Figure 8: Basic cells' coverage for without-centre-node topology.

Without-Centre-Node Basic Cell Coverage (in Transit Time Based Measurements)

In Figure 8, the basic-without-centre node cell is depicted.

For the Triangle the area (A_{T1} [m^2]) is expressed by Equation (5).

$$A_{T1} = \frac{(L)(L)(\cos 30°)}{2} = 0.5(L^2)\cos 30° \quad (5)$$

And for the Square the area (AS1 [m^2]) is calculated by Equation (6).

$$A_{S1}=L^2 \quad (6)$$

Triangular basic cells are combined in order to form the H-cell in Figure 9.

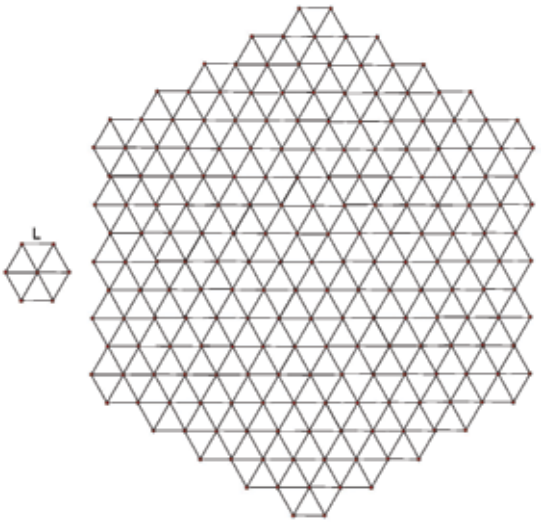

Figure 9: Hexagon cell's coverage consisting of without-centre-node basic cells. Red dots indicate transceivers. Left: one-layer H-cell consisting of seven transceivers. Right: five-layer network consisting of 211 transceivers.

With Triangles forming the Hexagon cell, the area of the Hexagon (A_{H1} [m^2]) is given by Equation (7).

$$AH_1 = \frac{3\sqrt{3}L^2}{2} \quad (7)$$

In the following section, without-centre-node cell combinations are investigated.

With-Centre-Node Basic Cell Coverage (in Modified Measurement Technique with the Calibration Phase Added)

As can be seen in Figure 9, in the new with-centre-node topology, the inter-node distance is considered the distance between the centre node and each vertex. Therefore, this topology has a larger area which is expressed by the Equations (8-12).

According to Figure 10, the Triangle's area (AT2 [m^2]) is expressed by Equation (8).

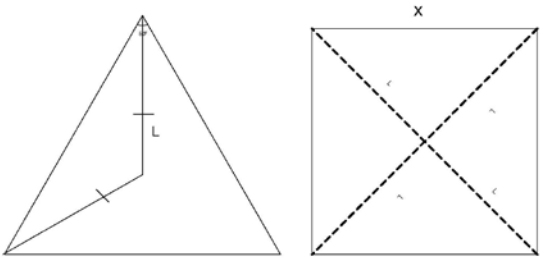

Figure 10: Basic cell coverage for with-centre-node topology.

$$A_{T2} = \frac{(L)(1+\sin(30°))(2(L)\cos(30°))}{2} = 1.5(L^2)\cos(30°) \quad (8)$$

In order to calculate the edge in the Square (X [m]), Equation (9) yields Equation (10) for the area of the S-cell (A_{S2} [m^2]) with-centre-node.

$$X = \sqrt{2}L \quad (9)$$

$$A_{S2} = 2L^2 \quad (10)$$

If the Triangle cells with-centre-node form the H-cell with-centre-node, as in Figure 11, its edge (X [m]) is given by Equation (11) and its

area (A_{H2} [m^2]) by Equation (12).

$$X = \sqrt{3}L \quad (11)$$

$$A_{H2} = \frac{3\sqrt{3}x^2}{2} = \frac{9\sqrt{3}L^2}{2}\ [m^2] \quad (12)$$

Coverage Comparisons

According to Equations (5)-(14), the coverage of the with-centre-node and without-centre-node configurations can be compared as shown below. Equation (13) shows that the with-centre-node Hexagonal design covers a three times bigger area than the design without-centre-node.

$$\frac{AH_2}{AH_1} = \frac{0.5\,(L^2)\cos(30°)}{1.5\,(L^2)\cos(30°)} = \frac{\frac{9\sqrt{3}L^2}{2}}{\frac{3\sqrt{3}L^2}{2}} = 3 \quad (13)$$

Similarly, for the Square design, the topology consisting of big Square cells (with-centre-node) covers an area two times bigger than the one consisting of basic Square cells (without-centre-node). This is calculated by Equation (14).

$$\frac{AS_2}{AS_1} = \frac{2L^2}{L^2} = 2 \quad (14)$$

As can be seen, if the centre node is added to the basic cells of the network, the modified architectures can cover a larger area in both the Hexagonal and Square topologies. This means that by applying the calibration phase in the current measurement process, instead of using just the traditional transit time method, it can result in a better coverage performance of the network.

The next section compares node density in the networks, which is a crucial factor affecting energy consumption.

Energy Consumption

In this section, it is shown that for bigger scales of underwater sensor networks, the extended coverage correlates with less node density and consequently lower energy consumption. The methodology used here for evaluating the networks' energy consumption is that the size (number of nodes) of each network can be calculated, which is done in the tables. Following the tables, formulations describe the performance of each design.

Energy Consumption in Hexagon Topology

For the Hexagonal topology, Table 1 shows the size of the without-centre-node configuration once a layer is added the network.

In Table 1 (according to Figure 9), the reason that the numbers of H-cells in column two are broken and not expressed as one number is that the number of nodes which are added to the H-cells are not the same for all H-cells, e.g., some H-cells take four added nodes while some others take three (the third column shows the number of nodes relating to the

Number of layers (L)	Number of Hexagon cells in each layer (H_1)	Number (coefficient) of added nodes/H-cell	Total number of transmitter nodes in the network of L layers: without-central-node (N_{T1})
1	1	7	7
2	6	4	7+(4)(6)=7+24=31
3	6+6	4-3	31+(4)(6)+(3)(6)=31+42=73
4	6+12	4-3	73+(4)(6)+(3)(6)+(3)(6)=73+60=133
5	6+18	4-3	133+(4)(6)+(3)(6)+(3)(6)+(3)(6)=133+78=211

Table 1: Hexagon network without-centre-node.

previous column). And this is why two different numbers are multiplied and added together in the fourth column. As an example, according to the second and third columns of the third layer-row, 4-3 means that six H-cells take four added nodes and six others take three. It should be mentioned that the redundant nodes are eliminated (as in Figure 9) and are not counted.

The next goal is to show that networks that are built from with-centre-node H-cells have fewer number of nodes per unit area (node/m^2) and therefore a larger area is covered with fewer acoustic sensors which results in less energy consumption. Likewise, as the deployment of the sensors in water is very difficult and expensive as well as their required maintenance, the with-centre-node configuration also effectively reduces the costs and hassles of the network. For the network of H-cells with-centre node, the total number of transmitter nodes is demonstrated in Table 2.

Number of layers (L)	Total number of H-cells (H_2)	Total number of transmitter nodes in the network of L layers: with-central-node (N_{T2})
1	1	3
2	7	21
3	19	57
4	37	111
5	61	183

Table 2: Hexagon network with centre node.

Also, the reason that the whole multiplication is broken into smaller building blocks of six (e.g., in four-layer row 12 in the second column breaks into two blocks of 6, multiplied by the relevant coefficients (four or three)) is to derive a closed-form formula (sum form) for the total number of added nodes in each layer.

Now for deriving a closed-form formula for the total added nodes in each layer, according to Table 1, the number of layers is considered as L, total added number of nodes in each layer as $N_{TI}(L)$, and the coefficients four and three as a and b, respectively. The first layer always has seven nodes (including the node in centre of the H-cell which is the vertex of all the basic cells combined). The others obey Equation (15) as below:

$$N_{TI}(L) = \begin{cases} 7, L = 1 \\ (a)(6) + (L-2)(b)(6) + n_1 \end{cases}$$

$$(L-1), L > 1 \quad while\ a = 4, b = 3 \qquad (15)$$

Equation (16) gives the number of transmitter nodes in with-centre-node Hexagonal configuration.

$$N_{T2}(L) = (3)H_2(L) \qquad (16)$$

It is very important to state that the key difference in the with-centre-node configuration and the without-centre-node is that in the former only the centre nodes are transmitters but in the latter all nodes need to be a transmitter at least once for each round of the measurement. As the transmitter nodes are the main consumers of the power in an underwater environment, it is obviously shown that the with-centre-node configuration has considerably lower node density than the other design and therefore uses less power.

The first column in Table 2 (according to Figure 11) is the number of layers *L*, the second one represents the number of cells which is basically the addition of the previous cells in the second column in Table 1, and the third column represents the total number of transmitter nodes in with-centre-node topology.

In the following section the Square topology is evaluated and compared with Hexagonal design.

For the network with big S-cell configuration, which is formed by with-centre-node basic cells, Table 4 and Equation (18) can yield the number of transmitters.

$$N_{S2} = \text{roundup}\left(\frac{((L)(L-1))^2}{2}\right) \quad (18)$$

In Equation (18), N_{S2} is the total number of transmitter nodes in the network and *L* represents the number of layers.

Layer (L)	Total number of S-cells	Nodes added/each layer (S_1)	Total number of transmitter nodes in the network of L layers: without-central-node (N_{S1})
1	1	(4)(1)=4	4
2	9	(4)(3)=12	16
3	25	(4)(5)=20	36
4	49	(4)(7)=28	64
5	81	(4)(9)=36	100

Table 3: Square network without-centre-node.

Layer	Total number of cells	Total transmitter nodes in the network of L layers: with-central-node (N_{S2})
1	1	1
2	9	5
3	25	13
4	49	25
5	81	41

Table 4: Square network with centre node.

Energy Consumption in Square Topology

For the without-centre-node Square topology, Table 3 and Equation (17) give the number of transmitter nodes.

The number of added nodes is shown by S_1, the total number of nodes by N_{S1}, and *L* is the number of layers.

$$S_1(L)=(4)(L + (L-1)) \quad (17)$$

$$N_{S1}(L)=S_1(L)+N_{S1}(L-1)$$

Node Density

As mentioned earlier, node density gives the final benchmark for the network designs and indicates which network consumes less energy. In order to calculate this parameter for each of the above architecture designs, Equation (19) has been used in the simulations, which is simply the result of a division of the total number of transmitters at each layer by the total area of coverage achieved by adding each level of the layers. In Equation (19), as in all other equations in this section, *L* represents the number of layers.

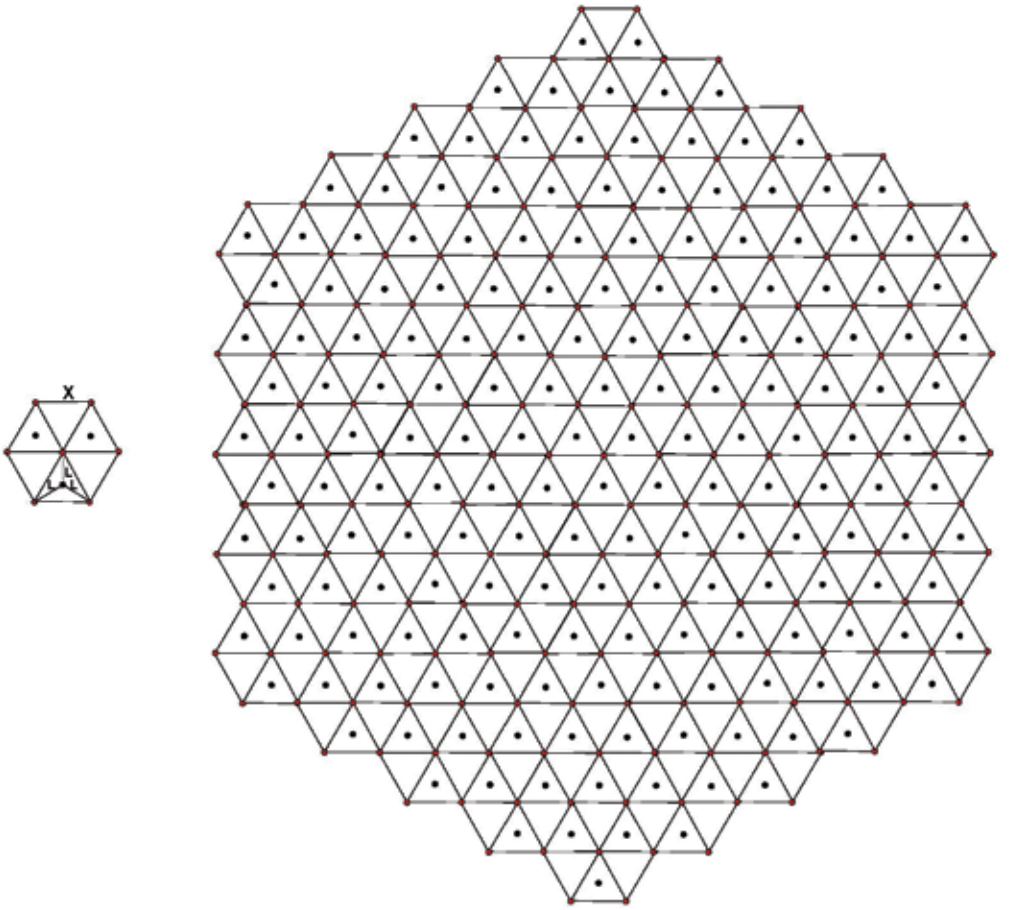

Figure 11: Hexagon cell coverage consisting of with-centre-node basic cells topology. Black dots are transmitters that are consider in energy consumption; red dots are only receivers. Left: one-layer H-cell consisting of three transmitters. Right: five-layer network consisting of 183 transducers.

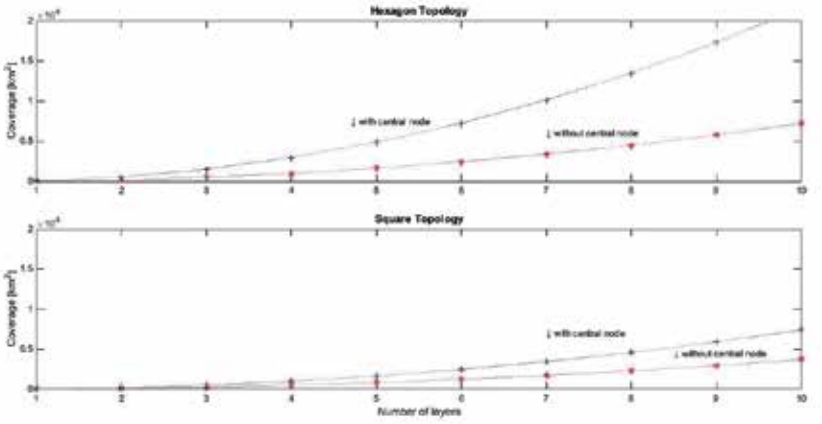

Figure 12: Coverage curves for with- and without-centre-node configurations. Top: Hexagon topology. Bottom: Square topology.

Node-density(L)=number of transmitter nodes(L) /A(L) (19)

As a result, the efficiency can be computed which is defined as the ratio of the *covered area* to *total number of nodes*. Thus in order to compare the efficiency of each two configurations, one's efficiency is divided by the other one. Equation (20) is an example explaining this comparison between the big Square topology, formed by with-centre-node configuration, and the basic Square cells topology, formed by without-centre-node configuration: (*area /nodes in Square with-centre node*) / (*area /nodes in Square without-centre node*)). In Equation (20), S_1 represents Square network without-centre node and S_2 represents Square network with-centre-cell.

$$\eta_{S2\_S1} = \frac{A_{S2}/A_{S1}}{Number\ of\ transmitters_{S2}/Number\ of\ transmitters_{S1}} \quad (20)$$

In Figures 12 to 15 network comparisons are depicted. The first graphical comparison is the networks' coverage depicted in Figure 12. Equation (21) is the one that has been used in the simulations which computes the area that has been covered with adding each layer to the network. In Equation (21), $A(L)$ [m^2] represents the area covered by L layers of network and A_{cell} [m^2] is the area of a single basic block cell forming the whole network.

$A(L) = (A_{cell}\ )$ (Total number of cells (L)) (21)

Figure 12 shows that with-centre-node configuration covers a larger area than without-centre-node configuration in both topologies. Also, the same number of layers in Hexagon topology covers a bigger area than the Square configuration.

Next is Figure 13 in which node density of the network is depicted by using Equation (20). Figure 13 shows that in Square topology the node density is slightly less than in the Hexagon configuration. This is an important indication that shows less power is consumed in with-centre-node Square type network, though, efficiency curves in Figures 14 and 15 show the effect of network design on power consumption more clearly.

Figure 14 compares an important specification of the designed architectures that is the efficiency of the designs. Figure 14 is comparing the with-centre-node configuration's efficiency to without-centre-node's using Equation (20).

As it can be seen in Figure 14, and according to the definition of efficiency that was previously mentioned, the efficiency of with-centre-node is better than without-centre-node design and by increasing the number of layers it converges to a constant number for both designs. Figure 14 also shows that the Square topology has a better efficiency than the Hexagon topology in general. Furthermore, it can be seen in Figure 14 that adding the centre node improves the efficiency of the network more than it does for the Hexagon configuration.

Figure 15 is another efficiency demonstration of Square design compared to the Hexagon each being in with- or without-centre configurations.

Figure 15 shows that in both with- and without-centre-node configuration, Square

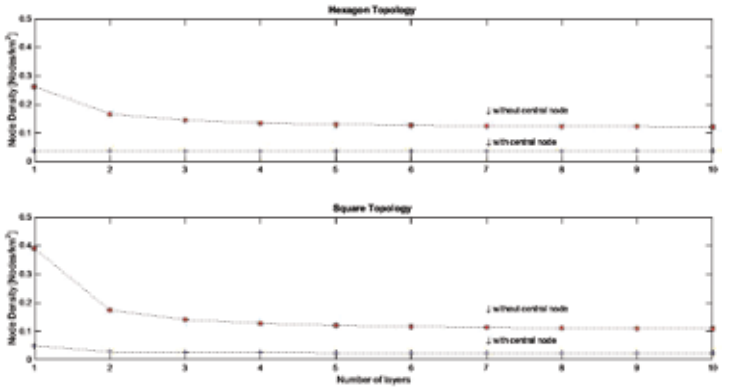

Figure 13: Node density curves for with- and without-centre-node configurations. Top: Hexagon topology. Bottom: Square topology.

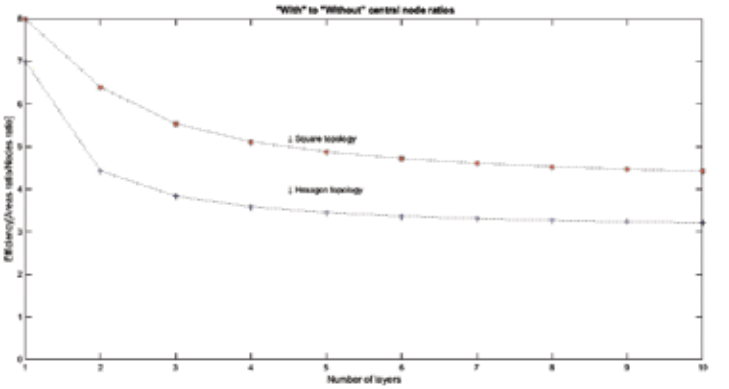

Figure 14: Efficiency ratio of with- to without-centre-node configuration.

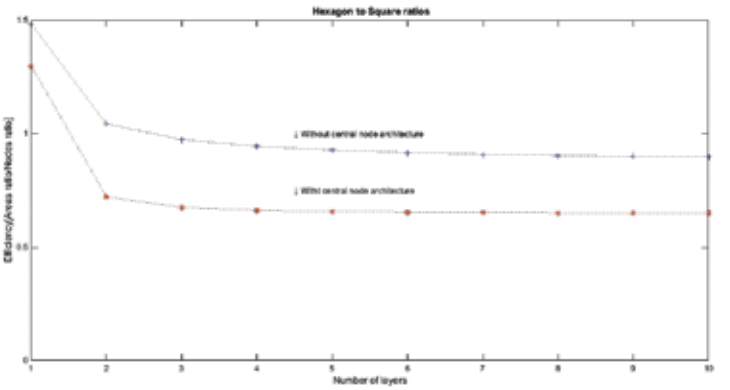

Figure 15: Efficiency ratio of Hexagon to Square topology.

topology has fewer nodes-per-area (especially in networks with more number of layers) and consequently is more efficient. Figure 15 actually confirms the results of Figure 14.

In order to summarize and according to Figures 12-15 and Tables 1-4, which are presented above, it is concluded that networks of the with-centre-node type can cover a larger area at sea with a fewer number of nodes than the without-centre-node configurations. Consequently, the new modified method that has been presented in this paper can yield a better efficiency result than the traditional transit time method.

Uncertainty

Lee et al. [2014] conducted laboratory and field experiments using StreamPro ADCP [RDI, 2008] for uncertainty analysis of velocity measurement. Their result shows +4.55% and +5.24% of uncertainties in the measurements done in laboratory and field conditions, respectively. These results are greater than the uncertainty specified by RDI for the instrument which is +1% or +2 mm/s. Comparing the uncertainty values reported by Lee et al. with the RDI value shows that the environmental conditions of the measurement affect the uncertainty value. This difference might exist in the uncertainty analysis of the proposed method in this paper as well. In the conditions under which the proposed method has been developed (see Appendix for more details), a

measurement uncertainty of +2% in a long range (scale of kilometres) could be achievable. Therefore, the uncertainty of the proposed technique in this paper is comparable with the uncertainty of measurements with the ADCP. However, in practice and with different sets of instruments (similar to the ones reported for StreamPro by Lee et al.) the uncertainty might be different. Hence some other criteria are needed to be imposed on the instruments in order to obtain the same value for the velocity measurement uncertainty.

CONCLUSION

In this paper, UASNs have been designed for ocean current measurements and theoretical analyses of the designs have been provided. The measurement technique in the proposed networks is based on propagation of a sound wave through a horizontal layer of ocean and measurement of transit time. It uses the transit time method for obtaining the speed of the sound in water. The speed of sound, which is computed in the calibration phase, is considered to be constant for only a short period of time when the current measurement phase is active and also is only considered to be constant in a limited zone at sea. The spatial distribution of the area where the speed of sound is considered constant (the constant speed zone extent) can vary depending on the required accuracy of the measurements. Having the underwater speed of sound and knowing the distances between the nodes (using GPS devices at each node) the ocean current can be measured.

The novel design of the UASNs is assessed in terms of energy consumption and the area they cover. It is shown that the modification of the transit time method helps in minimizing energy consumption in the whole network as well as the increase in the area of coverage. Therefore, the novel developed technique along with the new network designs would make considerable progress in provision of accurate and sustainable measurement of the real-time ocean current data or other underwater environmental factors.

APPENDIX: UNCERTAINTY ANALYSIS

For a given value of +2% for the uncertainty of the velocity measurements ($\frac{\Delta V}{V}\%$), Equations A1-A5 are used to calculate the limits for the uncertainty of the time measurement with the instruments used in the measurement process. These calculations assure that with the equipment used in our design, the desired velocity measurement uncertainty is achievable. The time measured by the transducers in the proposed method is shown by t in (A1). The distance between the transceivers is shown by d, C is the sound speed underwater, and v is the velocity of the water.

$$t = \frac{d}{c \pm v} \tag{A1}$$

By differentiating the two sides, error in the time measurement (Δt) and then time uncertainty ($\frac{\Delta t}{t}$) is given:

$$\left(\Delta t = \left|\frac{\partial t}{\partial d}\right| \Delta d + \left|\frac{\partial t}{\partial V}\right| \Delta V + \left|\frac{\partial t}{\partial C}\right| \Delta C = \left|\frac{1}{C \pm V}\right| \Delta d + \left|\frac{\pm d}{(C \pm V)^2}\right| \Delta v + \left|\frac{-d}{(C \pm V)^2}\right| \Delta C\right)\Big|_{\text{divided by } (t)}$$

$$\frac{\Delta t}{t} = \left|\frac{1}{d}\right| \Delta d + \left|\frac{\pm 1}{C \pm V}\right| \Delta v + \left|\frac{-1}{C \pm V}\right| \Delta c \approx \frac{\Delta d}{d} + \frac{\Delta V / V}{C \pm 1} + \frac{\Delta C}{C \pm V} \tag{A2}$$

The second term in the right side of the equation (A2) ($\frac{\Delta V/V}{C\pm1}$) is small and negligible. The measurement error of the GPS device, used for measuring the location of the transducers, is considered to be 1.8 m (Δd=1.8m). If $t=\frac{d}{C\pm V}\sim\frac{3200}{1480\pm1}=2.162162$, then provided that $C=\frac{d}{2}\frac{t_1+t_2}{t_1.t_2}$ (measured by using transit time method to measure the C), ΔC can be calculated in (A3) in which t_1 and t_2 indicate the upstream and downstream time measurement [Attarsharghi and Masek, 2014].

Therefore, allowable uncertainty for time measurement with the given uV%=2% is then calculated by (A5)

$$\frac{\Delta t}{t}\approx\frac{\Delta d}{d}+\frac{\Delta V/V}{C/V\pm1}+\frac{\Delta C}{C\pm V}=0.000563+\frac{0.02}{1480}+$$

$$0.000566=0.001143 \quad \text{(A5)}$$

Therefore, in order to have an uncertainty of lower than 2% in the velocity measurement, the measurement process should be able to measure the acoustic waves' travelling time

$$\left(\Delta C=\left|\frac{d}{2}.\frac{t_1t_2-t_2(t_1+t_2)}{(t_1t_2)^2}\right|\Delta t_1+\left|\frac{d}{2}.\frac{t_1t_2-t_1(t_1+t_2)}{(t_1t_2)^2}\right|\Delta t_2+\left|\frac{1}{2}\frac{t_1+t_2}{t_1t_2}\right|\Delta d\right.$$

$$\left.=\left|\frac{d}{2}.\frac{1}{(t_1)^2}\right|\Delta t_1+\left|\frac{d}{2}.\frac{1}{(t_2)^2}\right|\Delta t_2+\left|\frac{1}{2}\frac{t_1+t_2}{t_1t_2}\right|\Delta d\right)\Big| \quad \textit{divided by } C=\frac{dt_1+t_2}{2\ t_1.t_2},\frac{\Delta t_1}{t_1}=\frac{\Delta t_2}{t_2}=u_t$$

$$\Rightarrow \underbrace{\left|\frac{d}{2}.\frac{1}{t_1}\right|\frac{\Delta t_1}{t_1}+\left|\frac{d}{2}.\frac{1}{t_2}\right|\frac{\Delta t_2}{t_2}}_{u_t}+\underbrace{\left|\frac{1}{2}\frac{t_1+t_2}{t_1t_2}\right|}_{\frac{1}{d}}\Delta d$$

$$\rightarrow t_1=\frac{d}{C+V}=\frac{3200}{1480+1}=2.160702, t_2=\frac{d}{C-V}=\frac{3200}{1480-1}=2.163624 \quad \text{(A3)}$$

Sampling interval of the analogue to digital converter of the microcontroller used in the experiment in Attarsharghi and Masek [2014] is 8μs which results in a time measurement uncertainty of

$$u_t=\frac{\Delta t_1}{t_1}=\frac{\Delta t_2}{t_2}\cong\frac{0.000008}{2.162162}\cong\frac{0.000008}{2.163624}\cong3.7\mu$$

(using transit time method). Thus, uncertainty in the process of sound speed measurement in the calibration phase is within the range given by (A4).

$$\frac{\Delta C}{C}=u_C=u_t+u_d=\frac{0.000008}{2.162162}+\frac{1.8}{3200}=3.7\mu$$

$$+0.0005625=0.000566 \quad \text{(A4)}$$

with an uncertainty of $u_t\leq0.11\%$. This margin for time measurement uncertainty is safe and achievable with the instruments used in the laboratory experiments. Actually we consider the sampling interval of the analog to digital converter (ADC) in the microcontroller used in Attarsharghi [2016], which is +8μs, as the error in the whole time measurement process. Although the actual ADC error would be +4μs we add another +4μs in order to include all other possible sources of errors for the time measurement such as the pulse per second inaccuracy of the GPS device as well as the internal reference clock error of the microcontroller itself (however, each of them might have an error in the scale of nanoseconds).

REFERENCES

AquaTrans [n.d.]. *Underwater acoustic dunking hydrophone transducer.* Retrieved from: www.dspcomm.com/products_aquatrans.html.

Attarsharghi, S. [2016]. *Design criteria and practical insights into an underwater current measurement system along with simulation results of a real-case scenario in the Northwest Atlantic Ocean*. Journal of Ocean Technology, Vol. 11, No. 1, pp. 94-116.

Attarsharghi, S. and Masek, V. [2014]. *Ocean current monitoring via cross-correlation technique and node synchronisation*. IEEE Oceans, St. John's, NL, Canada. Retrieved from: http://ieeexplore.ieee.org/xpls/abs_all.jsp?arnumber=7003049&tag=1.

Brekhovskikh, L.M. and Lysanov, Yu.P. [2003]. *Fundamentals of ocean acoustics, 3rd edition*. Springer Science and Business Media, ISBN 978-0-387-95467-7.

Dohan, K. and Maximenko, N. [2010]. *Monitoring ocean currents with satellite sensors*. Oceanography Vol. 23, No. 4, p. 94.

Eik, K. [2009]. *Iceberg drift modelling and validation of applied metocean hindcast data*. Cold Regions Science and Technology, Vol. 57, No. 2, pp. 67-90.

Etter, P.C. [2013]. *Underwater acoustic modeling and simulation.* CRC Press. ISBN 9781466564930.

Fossette, S.; Putman, N.F.; Lohmann, K.J.; Marsh, R.; and Hays, G. [2012]. *A biologist's guide to assessing ocean currents: a review*. Marine Ecology Progress Series, Vol. 457, pp. 285-301.

Han, G.; Zhang, C.; Shu, L.; Sun, N.; and Li, Q. [2013]. *A survey on deployment algorithms in underwater acoustic sensor networks*. International Journal of Distributed Sensor Networks.

Heidemann, J.; Stojanovic, M.; and Zorzi, M. [2012]. *Underwater sensor networks: applications, advances and challenges*. Philosophical Transactions of the Royal Society of London A: Mathematical, Physical and Engineering Sciences, Vol., 370, No. 1958, pp. 158-175.

Hu, T. and Fei, Y. [2010]. *QELAR: a machine-learning-based adaptive routing protocol for energy-efficient and lifetime-extended underwater sensor networks*. IEEE Transactions on Mobile Computing, Vol. 9, No. 6, pp. 796-809.

Jha, D.K.; Wettergren, T.A.; Ray, A.; and Mukherjee, K. [2015]. *Topology optimisation for energy management in underwater sensor networks*. International Journal of Control, Vol. 88, No. 9, pp. 1775-1788.

Jornet, J.M.; Stojanovic, M.; and Zorzi, M. [2010]. *On joint frequency and power allocation in a cross-layer protocol for underwater acoustic networks*. IEEE Journal of Oceanic Engineering, Vol. 35, No. 4, pp. 936-947.

Jurdak, R.; Lopes, C.V.; and Baldi, P. [2004]. *Battery lifetime estimation and optimization for underwater sensor networks*. IEEE Sensor Network Operations, Vol. 2006, pp. 397-420.

Lee, K.; Ho, H.-C.; Marian, M.; and Wu, C.-H. [2014]. *Uncertainty in open channel discharge measurements acquired with StreamPro ADCP*. Journal of Hydrology, Vol. 509, pp. 101-114.

Lynnworth, L.C. [2013]. *Ultrasonic measurements for process control: theory, techniques, applications*. Academic Press. ISBN: 0323138039, 9780323138031.

Mitra, U.; Choudhary, S.; Hover, F.; Hummer,

R.; Kumar, N.; Naryanan, S.; Stojanovic, M.; and Sukhatme, G. [2015]. *Structured sparse methods for active ocean observation systems with communication constraints*. Communications Magazine, IEEE, Vol. 53, No. 11, pp. 88-96.

NOAA National Oceanic and Atmospheric Administration [n.d.A.] *How does the ocean affect climate and weather on land?* Retrieved from: http://oceanexplorer.noaa.gov/facts/climate.html.

NOAA National Oceanic and Atmospheric Administration [n.d.B.] *Currents and Marine Life*. Retrieved from: http://oceanexplorer.noaa.gov/edu/learning/8_ocean_currents/activities/currents.html.

NOAA National Oceanic and Atmospheric Administration [n.d.C.]. *Deep ocean drifter*. Retrieved from: http://oceanservice.noaa.gov/education/tutorial_currents/06measure4.html.

Paduan, J.D. and Washburn, L. [2013]. *High-frequency radar observations of ocean surface currents*. Annual Review of Marine Science, Vol. 5, pp. 115-136.

RDI [2008]. *StreamPro ADCP guide*. Teledyne RD Instruments, Poway, CA. Retrieved from: www.otronix.com/kr/data/p03/StreamPro_ADCP_Operationa_Manual.pdf.

Tilak, S.; Abu-Ghazaleh, N.B.; and Heinzelman, W. [2002]. *Infrastructure tradeoffs for sensor networks*. Proceedings of the 1st ACM international workshop on Wireless sensor networks and applications.

Turnbull, I.D.; Fournier, N.; Stolwijk, M.; Fosnaes, T.; and McGonigal, D. [2015]. *Operational iceberg drift forecasting in Northwest Greenland*. Cold Regions Science and Technology, Vol. 110, pp. 1-18.

Urick, J.R. [1983]. *Principles of underwater sound*. McGraw-Hill, New York. ISBN-13: 9780070660878.

Xiao, Y. [2010]. *Underwater acoustic sensor networks*. CRC Press.

Xiaoyu, D.; Lijuan, S.; and Linfeng, L. [2013]. *Coverage optimization Algorithm based on sampling for 3D underwater sensor networks*. International Journal of Distributed Sensor Networks.